

Benchmarking BrachyDose: Voxel based EGSnrc Monte Carlo calculations of TG-43 dosimetry parameters

R. E. P. Taylor,^{a)} G. Yegin, and D. W. O. Rogers^{b)}

Ottawa Carleton Institute of Physics, Carleton University, Ottawa, Canada K1S 5B6

(Received 11 August 2006; revised 23 October 2006; accepted for publication 23 October 2006; published 10 January 2007)

In this study, BrachyDose, a recently developed EGSnrc Monte Carlo code for rapid brachytherapy dose calculations, has been benchmarked by reproducing previously published dosimetry parameters for three brachytherapy seeds with varied internal structure and encapsulation. Calculations are performed for two ^{125}I seeds (Source Tech Medical Model STM1251 and Imagyn isoSTAR model 12501) and one ^{103}Pd source (Theragenics Model 200). Voxel size effects were investigated with dose distribution calculations for three voxel sizes: $0.1 \times 0.1 \times 0.1 \text{ mm}^3$, $0.5 \times 0.5 \times 0.5 \text{ mm}^3$, and $1 \times 1 \times 1 \text{ mm}^3$. In order to minimize the impact of voxel size effects, tabulated dosimetry data for this study consist of a combination of the three calculations: $0.1 \times 0.1 \times 0.1 \text{ mm}^3$ voxels for distances in the range of $0 < r \leq 1 \text{ cm}$, $0.5 \times 0.5 \times 0.5 \text{ mm}^3$ voxels for $1 < r \leq 5 \text{ cm}$ and $1 \times 1 \times 1 \text{ mm}^3$ voxels for $5 < r \leq 10 \text{ cm}$. Dosimetry parameters from this study are compared with values calculated by other authors using Williamson's PTRAN code and to measured values. Overall, calculations made with BrachyDose show good agreement with calculations made with PTRAN although there are some exceptions. © 2007 American Association of Physicists in Medicine. [DOI: 10.1118/1.2400843]

I. INTRODUCTION

Yegin *et al.* have recently developed BrachyDose,¹ a Monte Carlo (MC) code for rapid brachytherapy dose calculations. This code represents a valuable step forward since it allows rapid (5 min or less) Monte Carlo dose calculations for prostate implants based on the well established EGSnrc^{3,4} code. The EGS Monte Carlo code has been used previously in brachytherapy applications,⁵⁻¹² however, this is the first EGS user code capable of modeling the more complicated geometries found in many brachytherapy seeds. Although Williamson's PTRAN^{13,14} code has been used for these applications for many years, it is valuable to have a completely independent code. BrachyDose has the added advantage of being able to model electron transport which is important for modeling miniature x-ray sources being developed for brachytherapy applications.^{15,16} In this study, electron transport is not done since at the energies relevant to the calculations here, the range of electrons is effectively zero and their energy can be considered to be deposited locally.

The dosimetry protocol outlined by the AAPM's Task Group 43^{17,18} recommends that investigators benchmark new MC codes by reproducing previously published dosimetry parameters for at least one widely used source. In this study, BrachyDose has been used to calculate comprehensive TG-43 dosimetry parameters for three sources with varied internal structure and encapsulation. Calculations are performed for two ^{125}I seeds (Source Tech Medical Model STM1251¹⁹⁻²¹ and Imagyn isoSTAR model 12501²²⁻²⁵) and one ^{103}Pd source (Theragenics Model 200^{8,10,11,26-28}).

The majority of MC derived brachytherapy dosimetry parameters, available in the literature have been calculated using Williamson's PTRAN^{13,14} MC code. Unlike PTRAN, BrachyDose calculates volume-averaged doses to voxels

rather than using a point kerma estimator. This makes it imperative that voxel size effects be considered. Both the STM1251 and Model 200 seeds have highly anisotropic dose distributions at small angles relative to the seed axis and thus make good candidates for benchmarking a voxel based Monte Carlo code like BrachyDose. To investigate the effect of voxel size on dosimetry parameters, calculations were made with three different voxel sizes. Dosimetry parameters from the three sets of calculations are presented and comparisons are made with data calculated by other investigators using PTRAN.

BrachyDose calculated dose rate constants, radial dose functions and anisotropy data have been tabulated for the three sources considered here. In a related study a comprehensive set of dosimetry data for 16 different seeds (12 ^{125}I and 4 ^{103}Pd) will be presented.

II. MATERIALS AND METHODS

A. BrachyDose code

BrachyDose^{1,2} is a new EGSnrc Monte Carlo user code capable of doing full brachytherapy prostate implant calculations in 5 min on a single CPU. BrachyDose may be used to do calculations for ^{192}Ir , ^{125}I , ^{103}Pd and miniature x-ray sources, the latter case requiring electron transport within the source only. The incorporation of Yegin's multi-geometry package²⁹ into the BrachyDose code allows all of these different sources to be modeled in detail. In order to study the effects of cross section uncertainties, BrachyDose also has the capability to scale the cross section of any material by a user-specified factor.

BrachyDose scores the collision kerma per history in voxels via a tracklength estimator. Due to the low energies in-

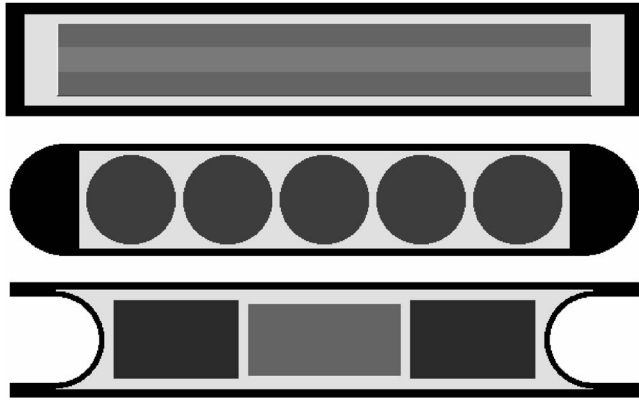


FIG. 1. Cross section of sources used in this study. Detailed descriptions of each source are given in the text. From top to bottom the sources are: (1) Source Tech Medical Model STM1251 (^{125}I), (2) Imagyn isoStar 12501 (^{125}I), (3) Theragenics Model 200 (^{103}Pd). Images were generated using MGview, a geometry visualization tool for Yegin's geometry package (Ref. 29). Sources are all drawn to scale (same scale for all sources).

involved, charged particle equilibrium can be assumed and collision kerma can be considered equal to the absorbed dose to the medium. Dose is calculated as

$$D^j = K_{\text{col}}^j = \sum_i E_i t_i \left(\frac{\mu_{\text{en}}}{\rho} \right)_i / V_j, \quad (1)$$

where D^j and K_{col}^j are the dose and collision kerma in the j th voxel, E_i is the energy of the i th photon, and t_i is the track-length of that photon in the voxel. The mass-energy absorption coefficient corresponding to energy E_i is $\left(\frac{\mu_{\text{en}}}{\rho} \right)_i$ and V_j is the volume of the voxel.

B. Brachytherapy sources

Source geometries including both encapsulation and internal structure were modeled using Yegin's multi-geometry package.²⁹ This geometry package gives users the ability to generate complex geometries composed of rectilinear, cylindrical, spherical and conical shapes. Figure 1 shows cross sections of the three seeds modeled in this study. The figures were generated using a separate code, MGview, which is part of the multi-geometry package.

The STM1251 ^{125}I source consists of a cylindrical gold rod with 0.18 mm diameter which is inside of 3.81-mm-long hollow aluminum wire with a diameter of 0.51 mm. The aluminum wire including the ends is coated with nickel (1.9 μm), copper (2.5 μm) and radioactive iodine (17 nm). The source is encapsulated in a titanium tube with 0.08-mm-thick walls, 0.81-mm-outer diameter and 0.13-mm-thick cylindrical end welds. All internal gaps are filled with air for all the seeds. The overall source length is 4.5 mm. These are the same dimensions used in the study by Kirov and Williamson.¹⁹

The Imagyn ^{125}I source consists of five silver spheres coated with AgI, encapsulated in a titanium tube with approximately hemispherical end welds. The tube has 0.05-mm-thick walls, a diameter of 0.8 mm and an overall length of 4.5 mm. The thickness of the AgI coating on the internal

spheres is not listed in any of the relevant references and is assumed to have negligible thickness in this study. There are inconsistencies in the literature regarding the dimensions of the silver spheres and the end welds for this source. Gearheart²² *et al.* report that the seed has 0.64 mm spheres and 0.5-mm-thick end welds while Nath and Yue²³ report 0.65 mm spheres and 0.6-mm-thick end welds. TG43U1 lists the diameter of the spheres as 0.56 mm and does not mention the weld thickness.¹⁸ Since comparisons are made with Gearheart *et al.*'s MC results, dimensions given in their paper were used in this study.

The Model 200 ^{103}Pd source consists of two cylindrical graphite pellets coated with radioactive palladium and separated by a cylindrical lead marker. The graphite cylinders have a diameter of 0.56 mm and a length of 0.89 mm. The lead marker is 1.09 mm long and 0.5 mm in diameter. The thickness of Pd on the graphite is 2.2 μm . The encapsulation for the Model 200 seed is a thin titanium tube that is 0.826 mm in diameter with wall thickness of 0.056 mm and length of 4.5 mm. The ends are sealed with hemispherical titanium end cups that are 0.04 mm thick. The dimensions are the same as those in Monroe and Williamson's³⁰ study.

C. Monte Carlo calculations

For the calculations in this study, electrons were not transported and the photon cutoff energy was set to 1 keV. Rayleigh scattering, bound Compton scattering, photoelectric absorption and fluorescent emission of characteristic x rays were all simulated. All calculations used photon cross sections from the XCOM³¹ database and mass energy absorption coefficients were calculated using the EGSnrc user-code g. Photon spectra recommended in TG-43U1 were used to sample incident photon energies and probabilities for both ^{125}I and ^{103}Pd . Up to 4×10^{10} histories were simulated in order to get 1σ statistical uncertainties of 2% or less at a distance of 10 cm for all sources.

Dose calculations were done with the source positioned at the center of a rectilinear water phantom (mass density of 0.998 g/cm^3) with dimensions of $30 \times 30 \times 30 \text{ cm}^3$ (effective radius of 18.6 cm). Melhus and Rivard³² have recently shown that a radius of 15 cm provides adequate scattering medium for calculating the radial dose function at 10 cm within $0.3 \pm 0.1\%$ and $1.1 \pm 0.2\%$ for ^{125}I and ^{103}Pd seeds, respectively. Dose distributions surrounding the source were scored in a grid of cubic voxels on the plane defined by the seed and transverse axis. To take advantage of the inherent symmetry of the geometry and reduce calculation times, dose values from the four identical quadrants of the scoring plane were averaged.

Calculations of the air kerma per history were scored *in vacuo*, avoiding the need to correct for attenuation by air. Mass energy absorption coefficients were calculated for air with the composition recommended by TG43U1 (40% humidity). In principle this is incorrect because air kerma standards always refer to dry air, but the difference is less than 0.01% at these energies. Characteristic x rays originating from the titanium encapsulation were suppressed by discard-

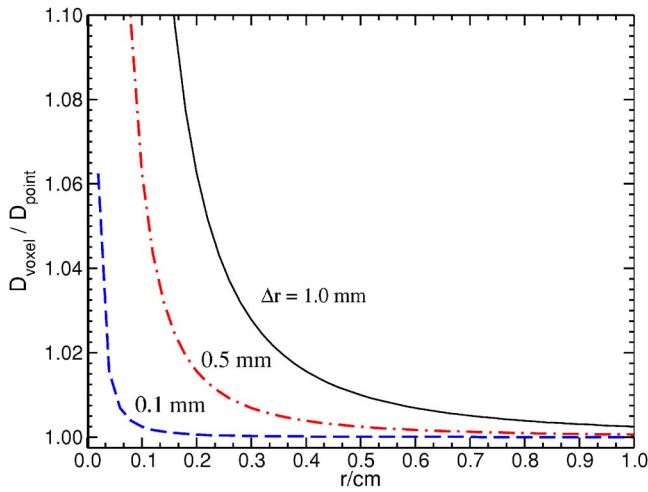


FIG. 2. Ratio of the average dose in spherical shells of thickness Δr [calculated using Eq. (5)] to dose at the midpoint of the shell for a point source with a $1/r^2$ distribution. Three different shell thicknesses are included. Scoring in shells of 1 mm thickness leads to dose overestimates of 2.8% and 0.25% at 3 and 10 mm, respectively. Decreasing the thickness of the shell to 0.1 mm leads to overestimates of less than 0.1% at the same two points.

ing fluorescent emissions with energies <5 keV, which in this case is equivalent to using a photon cutoff energy of 5 keV.

D. Voxel size effects

Dose scored in voxels is a volume averaged estimate of the dose at the center of a voxel. If the real dose distribution is given by $D(\mathbf{r})$ then the dose in a voxel, D_{vox} , scored in a volume ΔV is given by

$$D_{\text{vox}} = \frac{1}{\Delta V} \int_{\Delta V} dV D(\mathbf{r}). \quad (2)$$

For an arbitrary curve in one dimension, binned in intervals of width Δr , this expression can be written as

$$D_{\text{vox}} = \frac{1}{\Delta r} \int_{r_o - (\Delta r/2)}^{r_o + (\Delta r/2)} dr D(r). \quad (3)$$

Expanding using a Taylor series around the center of the bin, r_o , gives³³

$$D_{\text{vox}} = D(r_o) \left[1 + \frac{D''(r_o)}{24D(r_o)} \Delta r^2 + O(\Delta r^4) \right], \quad (4)$$

i.e., the calculated dose in the voxel represents the dose at the midpoint of the voxel when the second and higher order terms in Eq. (4) are negligible.

As a simple example, consider a point source with a dose distribution of $D(r) = \frac{D_o}{r^2}$ scored in spherical shells of width Δr . Equation (4) can be used to give the expression

$$D_{\text{vox}} \approx D(r_o) \left[1 + \frac{\Delta r^2}{4r_o^2} \right]. \quad (5)$$

Figure 2 shows the ratio of the dose scored in the voxel calculated using Eq. (5) to the point dose at the midpoint

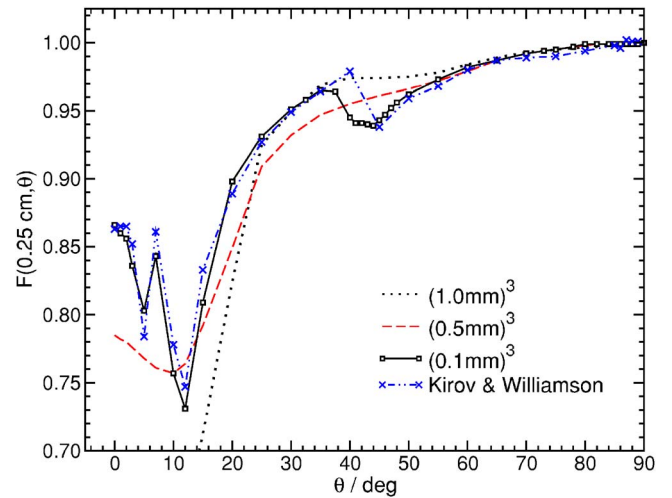


FIG. 3. Anisotropy function at $r=0.25$ cm for the STM12501 source. The plot shows the anisotropy function calculated with voxels of $(0.1 \text{ mm})^3$, $(0.5 \text{ mm})^3$ and $(1.0 \text{ mm})^3$ as well as values calculated by Kirov and Williamson (Ref. 19).

radius for three different shell thicknesses. For this simple case of a $\frac{1}{r^2}$ dose distribution, scoring in shells of 1 mm thickness leads to dose overestimates of 2.8% and 0.25% at 3 and 10 mm, respectively. Decreasing the thickness of the shell to 0.1 mm leads to dose overestimates of less than 0.1% at the same two points.

While the above isotropic example serves to illustrate the effect voxel size can have on calculated dose distributions, estimating the errors introduced by scoring dose in voxels surrounding brachytherapy seeds is less straightforward. The dose distribution surrounding a realistic seed may deviate greatly from $\frac{1}{r^2}$ due to the distribution of radioactive material within the seed and due to attenuation and scatter in the source and surrounding medium.

To investigate voxel size effects, dose distribution calculations were done with three voxel sizes: $0.1 \times 0.1 \times 0.1$, $0.5 \times 0.5 \times 0.5$, and $1 \times 1 \times 1 \text{ mm}^3$. Figure 3 is a plot of the anisotropy function of the SourceTech model STM1250 seed at $r=0.25$ cm calculated for the three different voxel sizes. It is apparent that calculations done with 1 and 0.5 mm voxels are not capable of calculating a realistic dose profile in this region. At a distance of 5 cm from the seed (Fig. 4), the anisotropy function at 0° calculated with 1 mm voxels is approximately 20% higher than the value calculated using 0.5 mm voxels. At an angle of just 1° the difference between the two calculations drops to 2%.

To minimize the impact of the voxel size effects discussed above, tabulated dosimetry data for this study consist of a combination of the three calculations. Voxel sizes were chosen in the following way: $0.1 \times 0.1 \times 0.1 \text{ mm}^3$ voxels were used for distances in the range of $0 < r \leq 1$ cm, $0.5 \times 0.5 \times 0.5 \text{ mm}^3$ voxels were used for $1 < r \leq 5$ cm and $1 \times 1 \times 1 \text{ mm}^3$ voxels were used for $5 < r \leq 10$ cm.

E. TG-43 dosimetry parameters

Data are tabulated as a function of distance from the seed and polar angle relative to the seed axis. When tabulation

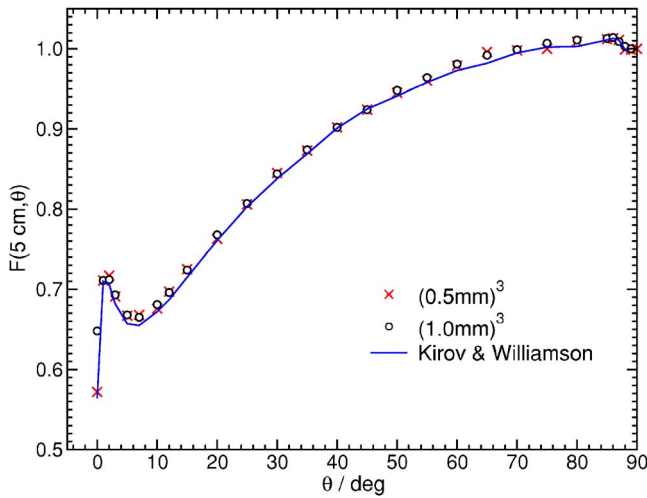


FIG. 4. Anisotropy function at $r=5$ cm for the STM12501 source. The plot shows the anisotropy function calculated with voxels of $(0.5 \text{ mm})^3$ and $(1.0 \text{ mm})^3$ as well as values calculated by Kirov and Williamson (Ref. 19). There is a significant voxel size effect at 0° only.

points do not correspond with the center of a voxel, dose values were interpolated bilinearly using the nearest neighbors of the voxel that the point of interest falls within. To improve the accuracy of the interpolation, all dose values were first divided by their respective values of the geometry function, $G_L(r, \theta)$. The geometry function is calculated using the line source approximation given by

$$G_L(r, \theta) = \begin{cases} 1/(r^2 - L^2/4) & \theta = 0 \\ \beta/Lr \sin \theta & \text{if } \theta \neq 0 \end{cases} \quad (6)$$

where the angle β ($=\theta_2 - \theta_1$ in TG-43 notation) is given by

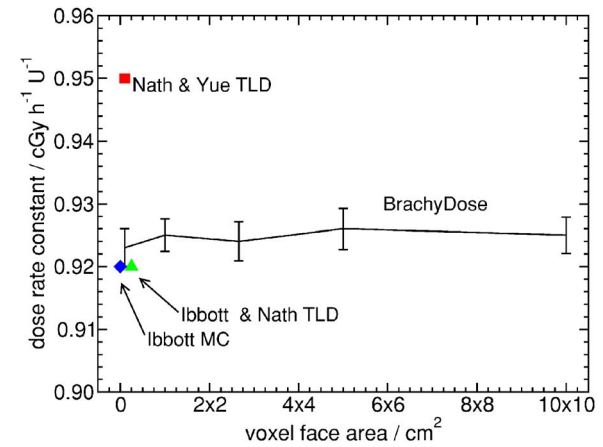


FIG. 6. As in Fig. 5 except for the Imagyn ^{125}I source. Ibbott *et al.*'s (Ref. 25) calculated value and TLD measurements (Refs. 22–24) are shown at 0 cm^2 . The reported uncertainty on the TLD measurements by Gearheart *et al.* (Refs. 22 and 24) and Nath and Yue are 7.7% and 10%, respectively.

$$\beta = \begin{cases} \tan^{-1}\left(\frac{Lr \sin \theta}{r^2 - L^2/4}\right) & r > L/2 \\ \tan^{-1}\left(\frac{Lr \sin \theta}{r^2 - L^2/4}\right) + \pi & r < L/2 \\ \pi/2 & r = L/2 \end{cases} \quad (7)$$

This geometry factor is equivalent to the definition given by TG-43U1 and is used here because it is faster to calculate.

Williamson *et al.* have shown^{19,27,30} that “Sources containing radioactivity deposited on radio-opaque surfaces with sharp corners give rise to distance- and angle-dependent self-shielding phenomena with surprising dosimetric results, including apparent inverse-square law breakdowns and significant anisotropy near the transverse axis.”²⁷ This anisotropy can lead to significant variations in the air kerma strength, and hence the dose rate constant, depending on whether the air kerma strength is scored at a point on the transverse axis

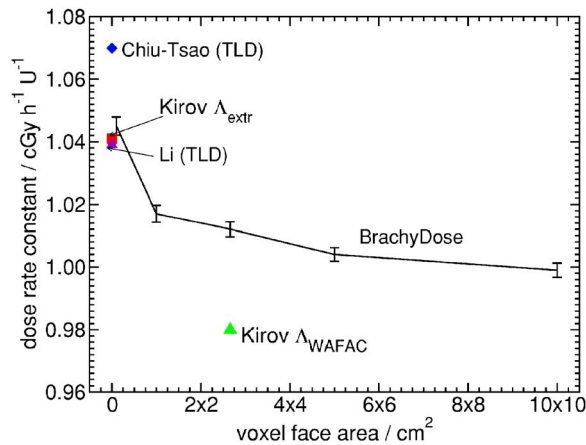


FIG. 5. Variation of the dose rate constant for the STM1251 ^{125}I seed as a function of the scoring volume for the air kerma strength per history. Dose rate constants were determined using air kerma strengths averaged over voxels that were 0.5 mm thick and faces with varying areas. The faces of the scoring voxels were located 10 cm from the source. For comparison, values of the dose rate constants calculated or measured by other authors (Refs. 19–21) are also included. The WAFAC calculation by Kirov and Williamson is shown at an area of $2.7 \times 2.7 \text{ cm}^2$. Kirov and Williamson's point kerma extrapolated estimate and TLD measurements are shown at 0 cm^2 . The reported uncertainties on Kirov's calculations, Li's measurements and Chiu-Tsao's measurements are 2.5%, 7% and 5.5%, respectively.

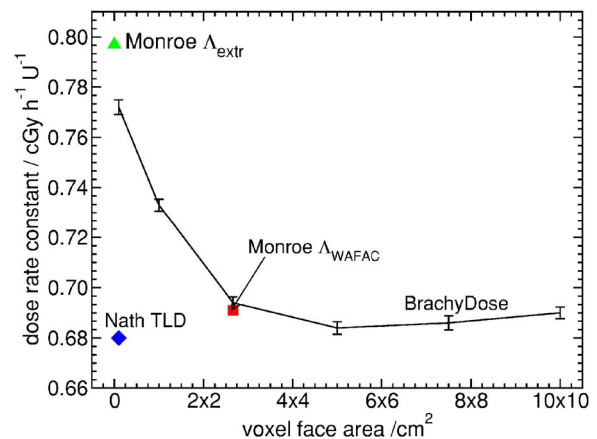


FIG. 7. As in Fig. 5 except for the Theragenics ^{103}Pd seed. The WAFAC calculations by Monroe and Williamson (Ref. 30) are shown at an area of $2.7 \times 2.7 \text{ cm}^2$. Monroe and Williamson's point kerma extrapolated estimate and Nath *et al.*'s (Ref. 28) TLD measurements are shown at 0 cm^2 . The reported uncertainties on Monroe and Williamson's MC results are 3%.

TABLE I. Dose rate constants, Λ , and uncertainties calculated in this study and from other authors. Uncertainties shown for the values calculated in this study are statistical uncertainties only and do not include uncertainties in cross section or geometry.

Seed name	Author	Method	Λ cGy h ⁻¹ U ⁻¹
STM12501	This study	2.7×2.7×0.05 cm ³ voxel at 10 cm	1.012±0.002
	This study	0.1×0.1×0.05 cm ³ voxel at 10 cm	1.045±0.003
	Kirov and Williamson ^a	MC (WAFAC sim.)	0.980±0.024
	Kirov and Williamson ^a	MC (pt. extrapolation)	1.041
	Li and Williamson ^b	TLD	1.039±0.073
	Chiu-Tsao ^c	TLD	1.07±0.06
Imagyn	This Study	2.7×2.7×0.05 cm ³ voxel at 10 cm	0.924±0.003
	This Study	0.1×0.1×0.05 cm ³ voxel at 10 cm	0.923±0.003
	Ibbott ^e	MC	0.92
	Gearheart <i>et al.</i> ^{d,f}	TLD	0.92±0.07
	Nath and Yu ^c	TLD	0.95±0.095
	TG-43 Consensus	Avg. of MC and TLD	0.940
Theragenics	This study	2.7×2.7×0.05 cm ³ voxel at 10 cm	0.694±0.002
	This study	0.1×0.1×0.05 cm ³ voxel at 10 cm	0.772±0.003
	Monroe and Williamson ⁱ	MC (WAFAC sim.)	0.691±0.02
	Monroe and Williamson ⁱ	MC (pt. extrapolation)	0.797
	Nath <i>et al.</i> ^h	TLD	0.680±0.05
	TG-43 Consensus	Avg. of MC and TLD	0.686

^aReference 19.

^bReference 20.

^cReference 21.

^dReference 22.

^eReference 23.

^fReference 24.

^gReference 25.

^hReference 28.

ⁱReference 30.

or averaged over a finite solid angle (as in the wide angle free air chamber (WAFAC) measurements performed at the National Institute of Standards and Technology (NIST)^{34,35}).

To investigate the influence of the photon fluence anisotropy on the determination of the dose rate constant, a number of calculations were done. The air kerma per history was scored in rectilinear voxels with the face of the voxel located 10 cm from the source. The voxels used for scoring air kerma per history were 0.5 mm thick and the area of the voxel's face was varied from 0.1×0.1 to 10×10 cm² (centered on the transverse axis). As a comparison, the NIST WAFAC primary collimator is 8 cm in diameter and is located 30 cm from the source. The primary collimator would subtend a circle with diameter of ~2.7 cm at a distance of 10 cm from the source.

Air kerma strength per history was calculated as

$$s_K = \dot{k}_\delta(d) \times d^2 \times k_{r,2}, \quad (8)$$

where \dot{k}_δ is the air kerma per history and d is the distance from the source to the face of the scoring voxel. The factor $k_{r,2}$ is the ratio of the average r^2 for the scoring volume to d^2 and is a correction to account for the variation of the inverse square law over the scoring region. This factor is used to give a result at a given distance which is independent of scoring volume size for a strictly point source and amounts to giving the air kerma per history $\times d^2$ on the axis. This correction factor can be calculated analytically as

$$k_{r,2} = \frac{1}{d^2 \cdot w^2 \cdot t} \int_d^{d+t} \int_{-w/2}^{w/2} \int_{-w/2}^{w/2} (x^2 + y^2 + z^2) dx dy dz, \quad (9)$$

where t is the thickness of the voxel (0.05 cm) and w is the width of the voxel (varied from 10 to 0.1 cm). At 10 cm from the source this amounts to a ~17.2% and 0.5% correction for the 0.05×10×10 and 0.05×0.1×0.1 cm³ voxels, respectively. The 10-cm-wide voxels are much larger than would be used in practice but are included here to demonstrate the dependence of the dose rate constant on the size of the region used for scoring air kerma.

Dose rate constants, Λ , are calculated as the dose to water per history in a (0.1 mm)³ voxel centered on the reference position (1 cm, $\frac{\pi}{2}$) in the 30×30×30 cm³ water phantom, divided by the air kerma strength per history.

The radial dose function, $g(r)$, is calculated using both line and point source geometry functions and tabulated at 1 mm intervals for distances less than 1 cm from the source and 0.5 cm intervals from 1 to 10 cm. Values at $r=0.25$ mm and $r=0.75$ mm are also included.

Anisotropy functions are calculated using the line source approximation and tabulated at radii of 0.25, 0.5, 0.75, 1, 2, 3, 4, 5, 7.5 and 10 cm. The same 32 polar angles used in Monroe and Williamson's study³⁰ of the Model 200 ¹⁰³Pd seed were used to provide high angular resolution near the transverse axis and seed axis. The anisotropy factor, $\phi_{an}(r)$, was calculated by integrating the solid angle weighted dose rate over $0^\circ \leq \theta \leq 90^\circ$ and the anisotropy constant, $\bar{\phi}_{an}$, was

TABLE II. Radial dose functions calculated using both line, $g_L(r)$, and point, $g_P(r)$, source approximations. Active lengths, L , used for calculating the geometry function are also provided. Uncertainties for the ^{125}I sources are approximately 0.5% for $r < 1$ cm, 0.7% at 5 cm and 1% at 10 cm. The uncertainties for the Theragenics source are approximately 0.5% for $r < 1$ cm, 1.0% at 5 cm and 2% at 10 cm.

Source name r/cm	$g_s(r)$					
	STM ^{125}I		Imagyn ^{125}I		Thera 200 ^{103}Pd	
	$L=3.8$ mm	Point	$L=3.4$ mm	Point	$L=4.2$ mm	Point
0.1	0.946	0.548	1.038	0.640	0.928	0.503
0.2	0.999	0.810	1.097	0.918	1.339	1.045
0.25	1.014	0.878	1.110	0.984	1.380	1.162
0.3	1.022	0.925	1.107	1.017	1.388	1.227
0.4	1.031	0.977	1.100	1.050	1.363	1.273
0.5	1.033	1.002	1.091	1.062	1.308	1.256
0.6	1.030	1.012	1.079	1.062	1.244	1.213
0.7	1.024	1.015	1.061	1.051	1.179	1.162
0.75	1.021	1.012	1.055	1.047	1.147	1.135
0.8	1.017	1.015	1.046	1.040	1.112	1.104
0.9	1.008	1.011	1.030	1.028	1.058	1.055
1.0	1.000	1.000	1.000	1.000	1.000	1.000
1.5	0.925	0.937	0.905	0.909	0.741	0.755
2.0	0.849	0.862	0.806	0.811	0.551	0.563
2.5	0.765	0.778	0.708	0.714	0.406	0.416
3.0	0.685	0.697	0.619	0.625	0.298	0.305
3.5	0.608	0.617	0.538	0.543	0.219	0.224
4.0	0.536	0.548	0.466	0.470	0.160	0.164
4.5	0.471	0.480	0.406	0.410	0.117	0.120
5.0	0.415	0.423	0.350	0.353	0.0865	0.0886
5.5	0.361	0.366	0.300	0.303	0.0635	0.0653
6.0	0.315	0.320	0.255	0.258	0.0469	0.0482
6.5	0.273	0.277	0.220	0.222	0.0345	0.0355
7.0	0.237	0.241	0.191	0.192	0.0256	0.0263
7.5	0.206	0.209	0.161	0.162	0.0193	0.0198
8.0	0.178	0.181	0.139	0.140	0.0147	0.0151
8.5	0.152	0.154	0.119	0.120	0.0112	0.0115
9.0	0.130	0.132	0.102	0.103	0.00837	0.00861
9.5	0.113	0.115	0.0886	0.0894	0.00641	0.00660
10.0	0.0976	0.0992	0.0736	0.0743	0.00513	0.00528

calculated as the inverse r -squared weighted average of $\phi_{\text{an}}(r)$ for $r \geq 1$ cm as recommended by TG-43U1.

III. RESULTS AND DISCUSSION

A. Dose rate constants

Figures 5–7 show the calculated dose rate constant versus the width of the scoring region used for the air kerma strength calculations. Variations of 4.6% in the dose rate constant are seen for the STM1251 source as the area of the air kerma scoring region is decreased from $10 \times 10 \text{ cm}^2$ ($\Lambda = 0.999 \pm 0.002 \text{ cGy h}^{-1} \text{ U}^{-1}$) to $0.1 \times 0.1 \text{ cm}^2$ ($\Lambda = 1.045 \pm 0.003 \text{ cGy h}^{-1} \text{ U}^{-1}$). The dose rate constant for the Imagyn source shows very little variation as the area of the air kerma scoring region is decreased from $10 \times 10 \text{ cm}^2$ ($\Lambda = 0.925 \pm 0.003 \text{ cGy h}^{-1} \text{ U}^{-1}$) to $0.1 \times 0.1 \text{ cm}^2$ ($\Lambda = 0.923 \pm 0.003 \text{ cGy h}^{-1} \text{ U}^{-1}$). The dose rate constant for the Theragenics ^{103}Pd source increased by 11% as the area of the scoring region was decreased from $10 \times 10 \text{ cm}^2$ ($\Lambda = 0.690 \pm 0.002 \text{ cGy h}^{-1} \text{ U}^{-1}$) to $0.1 \times 0.1 \text{ cm}^2$ ($\Lambda = 0.772 \pm 0.003 \text{ cGy h}^{-1} \text{ U}^{-1}$). Also shown on the plots are

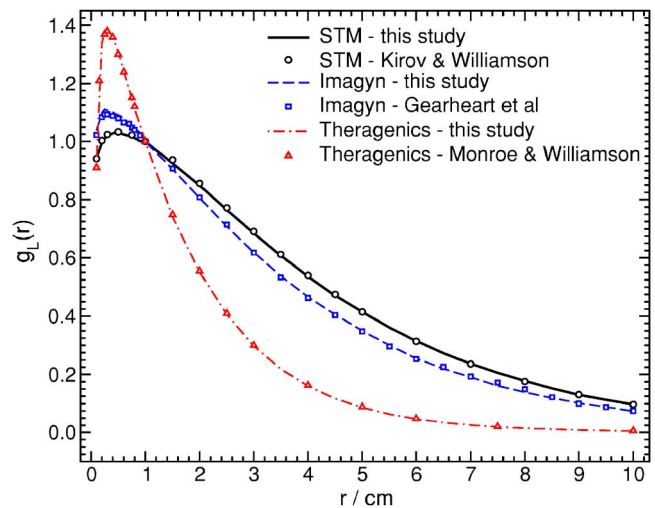


FIG. 8. Radial dose function $g_L(r)$, for the three sources. Voxel sizes are: $(0.1 \text{ mm})^3$ for $r \leq 1$ cm, $(0.5 \text{ mm})^3$ for $1 \text{ cm} < r \leq 5$ cm, $(1.0 \text{ mm})^3$ for $5 \text{ cm} < r \leq 10$ cm. Lines are values calculated in this study and symbols are values calculated by other authors (Refs. 19, 22, and 30).

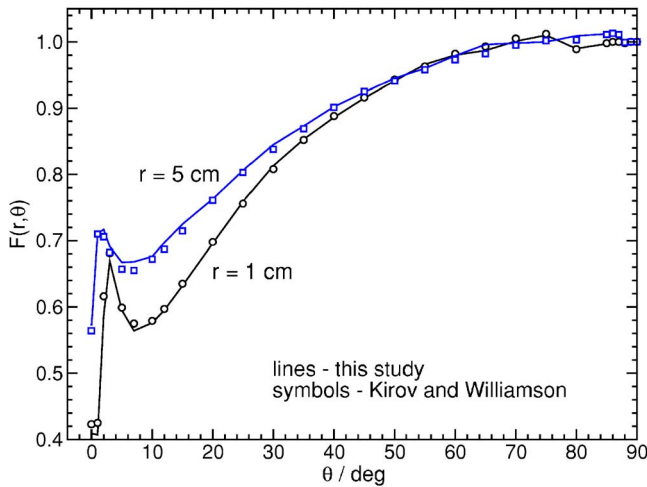


FIG. 9. Comparisons of anisotropy data calculated for the STM1251 ¹²⁵I source with values calculated by Kirov and Williamson (Ref. 19). Voxel sizes are (0.1 mm)³ at 1 cm and (0.5 mm)³ at 5 cm. See Fig. 3 for values at 0.25 cm.

relevant dose rate constants calculated or measured by other authors. For the STM and Theragenics sources, the dependence of the dose rate constant on the size of region used for scoring air kerma per history has been shown by Williamson *et al.*^{19,27,30} to be “a general feature of seeds containing internal components with sharp edges; composed of, or coated with, radio-opaque materials; and with radioactivity distributed on or near the surface.”³⁰ Since the Imagyn source uses spherical source elements, this same effect is not seen with this seed.

Calculated dose rate constants and their statistical uncertainties are listed in Table I. Included in the table are consensus dose rate constants recommended by TG-43U1 and/or relevant values calculated or measured by other authors. Our values in the table are based on the dose to water per history at 1 cm in a 0.1 × 0.1 × 0.1 mm³ voxel and air kerma per history values calculated using voxels of 2.7 × 2.7 × 0.05 cm³ (method 1) and 0.1 × 0.1 × 0.05 cm³ (method 2) located 10 cm from the source. The larger voxel size averages the air kerma per history over a region subtending

TABLE III. Anisotropy function, $F(r, \theta)$, and anisotropy factors, $\phi_{an}(r)$, for the STM1251 source calculated using the line source approximation with $L=3.8$ mm. Uncertainties are approximately 0.2%, 0.5% and 1% at 1, 5 and 10 cm, respectively.

θ (deg)	r (cm)	$F(r, \theta)$									
		0.25	0.5	0.75	1	2	3	4	5	7.5	10
0		0.865	0.514	0.432	0.409	0.462	0.514	0.550	0.571	0.665	0.691
1		0.860	0.505	0.427	0.410	0.593	0.665	0.693	0.711	0.722	0.730
2		0.856	0.481	0.500	0.581	0.654	0.702	0.712	0.711	0.716	0.729
3		0.836	0.547	0.644	0.659	0.657	0.672	0.685	0.688	0.694	0.718
5		0.804	0.659	0.601	0.587	0.608	0.633	0.655	0.661	0.682	0.693
7		0.843	0.588	0.559	0.560	0.597	0.629	0.651	0.664	0.685	0.701
10		0.756	0.564	0.560	0.571	0.613	0.646	0.668	0.676	0.698	0.707
12		0.731	0.578	0.580	0.590	0.631	0.662	0.682	0.693	0.706	0.720
15		0.808	0.617	0.619	0.628	0.666	0.695	0.715	0.723	0.740	0.742
20		0.898	0.693	0.689	0.695	0.724	0.746	0.758	0.762	0.775	0.779
25		0.931	0.760	0.753	0.757	0.775	0.792	0.808	0.804	0.810	0.824
30		0.950	0.816	0.805	0.807	0.820	0.834	0.843	0.846	0.843	0.845
35		0.964	0.864	0.851	0.849	0.859	0.869	0.876	0.872	0.875	0.883
40		0.945	0.904	0.889	0.885	0.891	0.899	0.904	0.899	0.899	0.904
45		0.943	0.934	0.921	0.916	0.918	0.923	0.929	0.923	0.925	0.929
50		0.962	0.956	0.948	0.942	0.941	0.948	0.952	0.944	0.940	0.936
55		0.973	0.972	0.968	0.963	0.962	0.965	0.966	0.960	0.952	0.957
60		0.981	0.984	0.981	0.979	0.979	0.980	0.985	0.978	0.973	0.969
65		0.987	0.994	0.992	0.990	0.990	0.994	0.999	0.996	0.983	0.983
70		0.992	0.974	1.001	0.998	1.000	1.002	1.004	0.998	0.992	0.979
73		0.995	0.983	1.005	1.003	1.004	1.010	1.012	1.001	0.991	0.988
75		0.996	0.988	0.998	1.005	1.005	1.011	1.010	1.005	0.997	0.987
78		0.997	0.993	0.987	1.007	1.008	1.013	1.018	1.007	1.005	1.002
80		0.998	0.994	0.991	0.987	1.010	1.014	1.014	1.009	1.004	1.004
82		0.999	0.996	0.996	0.991	1.011	1.014	1.019	1.006	0.999	0.998
84		0.999	0.997	0.998	0.995	1.008	1.015	1.017	1.009	1.007	0.996
85		0.999	0.998	0.999	0.995	1.000	1.015	1.017	1.011	1.001	1.000
86		0.999	0.999	0.999	0.998	0.994	1.011	1.021	1.013	1.004	0.999
87		0.999	0.998	0.999	0.997	0.995	1.001	1.015	1.013	1.001	1.009
88		0.999	0.998	0.999	0.998	0.995	0.999	1.003	1.001	0.999	1.001
89		1.000	0.999	1.000	0.996	0.997	0.999	1.002	1.000	1.001	0.998
90		1.000	1.000	1.000	1.000	1.000	1.000	1.000	1.000	1.000	1.000
$\phi_{an}(r)$		1.211	0.982	0.951	0.940	0.937	0.948	0.948	0.943	0.942	0.939

TABLE IV. Anisotropy function, $F(r, \theta)$, and anisotropy factors, $\phi_{an}(r)$, for the Imagyn source calculated using the line source approximation with $L=3.4$ mm. Uncertainties are approximately 0.4%, 0.7% and 1.4% at 1, 5 and 10 cm, respectively.

θ (deg)	r (cm)	$F(r, \theta)$									
		0.25	0.5	0.75	1	2	3	4	5	7.5	10
0		0.170	0.207	0.240	0.268	0.345	0.395	0.425	0.448	0.498	0.508
1		0.171	0.207	0.239	0.271	0.352	0.402	0.438	0.457	0.503	0.534
2		0.173	0.207	0.242	0.277	0.357	0.408	0.440	0.454	0.505	0.526
3		0.176	0.209	0.252	0.288	0.361	0.409	0.440	0.458	0.502	0.527
5		0.187	0.225	0.260	0.290	0.366	0.415	0.447	0.463	0.511	0.536
7		0.203	0.236	0.273	0.307	0.381	0.428	0.459	0.475	0.522	0.544
10		0.252	0.268	0.306	0.341	0.412	0.457	0.486	0.504	0.553	0.562
12		0.293	0.299	0.337	0.370	0.436	0.479	0.511	0.523	0.562	0.575
15		0.383	0.353	0.383	0.415	0.474	0.514	0.538	0.547	0.588	0.604
20		0.528	0.445	0.466	0.489	0.537	0.570	0.594	0.605	0.635	0.647
25		0.641	0.532	0.543	0.563	0.600	0.626	0.646	0.655	0.679	0.696
30		0.730	0.613	0.617	0.634	0.659	0.679	0.696	0.697	0.724	0.742
35		0.797	0.688	0.684	0.698	0.715	0.735	0.746	0.741	0.766	0.773
40		0.847	0.755	0.747	0.759	0.767	0.778	0.790	0.789	0.811	0.812
45		0.882	0.812	0.804	0.814	0.814	0.824	0.833	0.830	0.850	0.854
50		0.908	0.863	0.855	0.865	0.859	0.865	0.870	0.869	0.886	0.887
55		0.930	0.910	0.901	0.909	0.899	0.905	0.906	0.903	0.917	0.917
60		0.950	0.944	0.936	0.947	0.934	0.939	0.943	0.927	0.944	0.958
65		0.962	0.965	0.965	0.978	0.963	0.963	0.968	0.959	0.970	0.975
70		0.974	0.981	0.986	0.998	0.983	0.982	0.989	0.977	0.987	0.990
73		0.979	0.987	0.991	1.007	0.990	0.990	0.993	0.984	0.993	0.992
75		0.984	0.992	0.993	1.006	0.992	0.991	0.992	0.985	0.997	0.992
78		0.988	0.996	0.997	1.010	0.996	0.992	0.996	0.991	1.002	1.005
80		0.991	0.996	0.997	1.011	0.996	0.998	0.997	0.988	1.000	1.007
82		0.993	0.998	1.000	1.011	0.997	0.998	1.002	0.995	1.006	1.006
84		0.995	0.998	1.000	1.008	0.999	1.001	1.002	0.991	1.016	1.007
85		0.996	0.998	1.000	1.011	1.000	1.000	1.004	0.997	1.013	1.006
86		0.997	0.999	1.000	1.008	1.000	1.003	1.004	0.999	1.008	1.004
87		0.997	1.000	1.001	1.013	1.000	1.002	1.000	0.989	1.016	1.010
88		0.998	1.001	1.001	1.010	1.000	0.999	1.005	0.998	1.007	1.015
89		0.999	1.001	0.999	1.010	1.000	1.000	1.000	0.992	1.008	0.997
90		1.000	1.000	1.000	1.000	1.000	1.000	1.000	1.000	1.000	1.000
$\phi_{an}(r)$		1.024	0.886	0.868	0.873	0.867	0.874	0.881	0.877	0.894	0.898

roughly the same solid angle as subtended by the primary collimator of the WAFAC. The small voxel serves to estimate the air kerma per history at a point on the transverse axis. It should be noted that Williamson *et al.* have shown that for the Theragenics^{27,30} and STM¹⁹ sources, air kerma strength calculated at a point on the transverse axis is dependent on the distance of the point from the seed. As such, dose rate constants calculated using the small voxel (method 2) in this study may not be directly comparable to the point extrapolation method used in other studies of those two sources.

The dose rate constant calculated for the STM source using the large voxel (method 1) is 3.3% higher than the value calculated by Kirov and Williamson using a full simulation of the WAFAC. The source of this discrepancy has not been identified. Kirov and Williamson's dose rate constant based on a point extrapolated air kerma strength is in much better agreement (within 0.4%) with the value calculated in this

study using the small voxel (method 2). Agreement of the method 2 calculation with the value measured by Li and Williamson²⁰ is also within 0.6%.

Dose rate constants calculated for the Imagyn source showed very little dependence on the scoring region size. Dose rate constants calculated with the two methods described above agree with each other within 0.5%. Calculated values show agreement with the values calculated and measured by Gearheart *et al.*²² within 0.5%.

For the Theragenics source, the dose rate constant based on the WAFAC simulation calculated by Monroe and Williamson³⁰ is 0.4% lower than the value calculated in this study using the large voxel (method 1). Monroe and Williamson's dose rate constant based on their point extrapolated air kerma strength is 3% higher than the value calculated in this study using the small voxel (method 2). Again, this 3% difference for the method 2 calculation is not surprising as it has been demonstrated in other studies of the Model 200

TABLE V. Anisotropy function, $F(r, \theta)$, and anisotropy factors, $\phi_{an}(r)$, for the Theragenics source calculated using the line source approximation with $L=3.4$ mm. Uncertainties are approximately 0.3%, 1% and 2% at 1, 5 and 10 cm, respectively.

θ (deg)	r (cm)	$F(r, \theta)$									
		0.25	0.5	0.75	1	2	3	4	5	7.5	10
0		0.604	0.688	0.601	0.553	0.522	0.517	0.516	0.511	0.544	0.632
1		0.605	0.683	0.597	0.559	0.515	0.515	0.527	0.528	0.556	0.643
2		0.607	0.671	0.583	0.545	0.512	0.520	0.526	0.524	0.557	0.631
3		0.607	0.647	0.573	0.540	0.509	0.515	0.524	0.530	0.558	0.625
5		0.599	0.596	0.532	0.512	0.500	0.510	0.520	0.527	0.557	0.634
7		0.552	0.548	0.512	0.498	0.496	0.511	0.520	0.529	0.559	0.644
10		0.317	0.492	0.488	0.486	0.501	0.516	0.531	0.535	0.572	0.656
12		0.232	0.469	0.480	0.488	0.507	0.526	0.539	0.546	0.584	0.671
15		0.322	0.446	0.477	0.493	0.520	0.543	0.557	0.561	0.602	0.673
20		0.522	0.451	0.489	0.511	0.545	0.571	0.590	0.596	0.634	0.707
25		0.679	0.512	0.532	0.550	0.582	0.610	0.625	0.635	0.667	0.747
30		0.795	0.601	0.596	0.606	0.632	0.656	0.676	0.685	0.707	0.749
35		0.877	0.680	0.673	0.676	0.689	0.711	0.724	0.733	0.757	0.804
40		0.929	0.748	0.739	0.742	0.750	0.771	0.779	0.789	0.804	0.849
45		0.949	0.804	0.798	0.799	0.806	0.823	0.833	0.838	0.851	0.872
50		0.945	0.849	0.843	0.845	0.854	0.871	0.882	0.885	0.892	0.907
55		0.941	0.887	0.884	0.887	0.896	0.912	0.921	0.924	0.935	0.936
60		0.976	0.917	0.919	0.925	0.933	0.950	0.955	0.956	0.965	0.970
65		0.984	0.930	0.945	0.955	0.962	0.978	0.985	0.978	0.989	0.973
70		0.983	0.931	0.962	0.976	0.989	1.005	1.015	1.007	1.006	1.012
73		0.973	0.917	0.964	0.983	1.002	1.020	1.029	1.030	1.023	1.002
75		0.959	0.940	0.967	0.982	1.009	1.027	1.039	1.034	1.026	1.012
78		0.974	0.955	0.949	0.987	1.017	1.035	1.047	1.046	1.037	1.025
80		0.989	0.958	0.967	0.984	1.020	1.039	1.051	1.048	1.045	1.037
82		0.998	0.950	0.976	0.973	1.020	1.044	1.057	1.048	1.041	1.036
84		1.003	0.958	0.975	0.990	1.012	1.036	1.047	1.047	1.044	1.047
85		1.003	0.972	0.970	0.986	1.003	1.029	1.044	1.033	1.044	1.039
86		1.003	0.982	0.976	0.983	0.995	1.019	1.034	1.030	1.032	1.024
87		1.002	0.988	0.992	0.981	0.995	1.006	1.024	1.016	1.021	1.011
88		1.001	0.995	0.998	0.993	0.992	1.007	1.011	1.013	1.013	1.022
89		1.001	0.999	0.999	1.000	0.993	1.001	1.011	1.008	0.998	1.018
90		1.000	1.000	1.000	1.000	1.000	1.000	1.000	1.000	1.000	1.000
$\phi_{an}(r)$		1.142	0.889	0.867	0.865	0.871	0.888	0.899	0.899	0.907	0.923

source that the air kerma strength determined at a point on the transverse axis depends on the distance from the source.

In all comparisons with TLD measured values, it must be noted the authors have all assumed the detector reading was proportional to the dose in the TLD, whereas the results of Davis *et al.*³⁶ imply the reading is high by up to 10% (for a 30 kV x-ray spectrum) which suggests all previous measured values may be systematically up to 10% high, although the results of Davis *et al.* directly contradict the results of Das *et al.*³⁷ This area requires further investigation.

B. Radial dose functions

Radial dose functions calculated using both the line source and point source approximations are presented in Table II. Figure 8 shows plots of $g_L(r)$ calculated in this study as well MC data from other studies. Statistical uncertainties for the two ¹²⁵I sources are $\sim 0.5\%$ and $\sim 1\%$ at 5 and 10 cm, respectively, while uncertainties for the Theragenics source are $\sim 1\%$ and $\sim 2\%$ at 5 and 10 cm, respectively.

The radial dose function calculated for the STM source in this study agrees within 1% with the values calculated by Kirov and Williamson¹⁹ at all distances. For the Imagyn source the radial dose function is approximately 1% higher than the values reported by Gearheart *et al.*²² for $r < 1$ cm. For $1 < r < 5$ cm agreement is within 1%, with the values calculated in this study being slightly greater than Gearheart *et al.*'s. For $5 < r < 10$ cm there is no obvious trend in the differences between the two calculations. There is a difference of close to 7% at $r=8$ cm but calculations are within 2% at 10 cm. These differences likely reflect the 4% statistical uncertainty reported for the value of Gearheart *et al.* for the radial dose function.²²

Agreement with the calculations of Monroe and Williamson³⁰ for the Theragenics ¹⁰³Pd source is better than 1% for $0.1 < r < 3$ cm, however, there are some significant differences at distances beyond 3 cm. Values calculated at 5, 7.5, and 10 cm in this study are lower than the values calculated by Monroe and Williamson by 2.5%, 6% and 16%, respectively. Monroe and Williamson state that uncertainties

on their calculations are $\sim 2\%$ at distances far from the source, making it unlikely that the differences are statistical in nature. Radial dose functions were also calculated for an unencapsulated point source and compared with values calculated by Monroe and Williamson and by Melhus and Rivard.³² Agreement between these three sets of calculations was within 1% for $r \leq 10$ cm demonstrating that the differences in radial dose functions originate in modeling the source.

To investigate the sensitivity of the results to cross sections, the radial dose function was recalculated with the cross section of Pd reduced by 5%. While the absolute dose rate increased by 0.6% at the reference position, (1 cm, 90°), the re-calculated radial dose function agreed with the standard calculation within statistical uncertainties for distances less than 10 cm from the source. The differences between the radial dose function calculations in this study and Monroe and Williamson's are unexplained given the good agreement for the dose rate constant (see Fig. 7) and anisotropy functions (see Fig. 11 below).

C. Anisotropy data

Calculated anisotropy data including the anisotropy factors for all sources are shown in Tables III–V. The anisotropy constants calculated in this study are shown in Table VI. Figures 9–11 show anisotropy function data for the three sources calculated at 1 and 5 cm as well as anisotropy data published by other authors.

For the STM source (Figs. 3 and 9), agreement with Kirov and Williamson's¹⁹ calculations is generally better than 1%. However, larger differences of $\sim 6\%$ are seen for $\theta = 2^\circ$ at $r = 1$ and 2 cm (2 cm data not shown) but these points are in regions of very steep dose gradients and good agreement is seen a short distance away. The anisotropy factors and constant are all in agreement within 1% for the STM source.

For the Imagyn source (Fig. 10), our anisotropy data with $\theta \geq 20^\circ$ generally agree within 2% with the values published by Gearheart *et al.* At 10° the anisotropy function values calculated in this study are 4% higher than those calculated by Gearheart *et al.*²² and at 0° the discrepancy is as large as

11% for $r = 1$ cm. Anisotropy factors agree within 2% and anisotropy constants are within 0.1% of each other.

The discrepancies in our $F(r, 0^\circ)$ values and those of Gearheart *et al.*²² of up to 11% for the Imagyn source at 0° do not appear to be caused by voxel size effects. Figure 11 is a plot of dose profiles for the Imagyn IS-12501 source taken perpendicular to the seed axis and offset 0.5 cm from the source center. This figure shows the shadowing effect that the end cap of the source encapsulation has (diameter of 0.8 mm) and that the dose profile is relatively flat within the shadow. Decreasing the voxel size even further should have little effect on the dose values calculated near the source axis. Also shown are calculations done with $0.5 \times 0.5 \times 0.5$ mm³ voxels. The dose calculated in the two voxel sizes is the same within uncertainties at 0° .

Since this region of space is where photons undergo the most significant attenuation by the encapsulation, the discrepancy between this study and previous studies may result from differences in the photon cross sections used. Gearheart *et al.* used the DLC-99³⁸ cross sections while all calculations for this study were done using XCOM cross sections.³¹ To investigate the impact of cross section uncertainties a set of calculations for the Imagyn source was done in which the cross sections of the Ti encapsulation were increased by 1%.

Figure 12 shows the ratio of dose calculated with the standard cross section to the dose calculated with the increased cross sections for Ti. Again the dose profiles for this plot were taken perpendicular to the seed axis and offset 0.5 cm from the source center. Increasing the cross section of Ti by 1% led to a decrease of dose of close to 0.8% at 0.5 cm along the seed axis. At 0.5 cm along the transverse axis the decrease in dose was only 0.2% giving a decrease in the anisotropy function of $0.53 \pm 0.14\%$ at $(r, \theta) = (0.5 \text{ cm}, 0^\circ)$. Discrepancies between the two calculations decreased as the distance from the source and polar angles increased. No significant differences were seen in the radial dose function for the two calculations. These calculations show that differences in cross sections on the order of 1% lead to significant differences in calculated anisotropy function data. We can therefore deduce that a large discrepancy ($> 1\%$) in cross section data may lead to large differences in calculated anisotropy data and may be the cause of the discrepancy between $F(r, 0^\circ)$ values calculated in this study and those of Gearheart *et al.*²²

The Theragenics seed's anisotropy data (Fig. 13) show very good agreement with the data calculated by Monroe and Williamson.³⁰ The anisotropy function agrees within 1%–2% at almost all angles and radii considered, with the one notable exception being for $r = 0.25$ cm and $7^\circ \leq \theta \leq 20^\circ$ where there are discrepancies of 5% or more. This is the region which has the steepest dose gradients and undergoes the most significant attenuation due to the structure of the seed. At 12° and 0.25 cm the anisotropy function value calculated in this study is 20% higher than that calculated by Monroe and Williamson while at 12° and 0.5 cm the difference has dropped to less than 1%. These differences are in regions where voxel size effects are most pronounced and are most

TABLE VI. Tabulated values of the one-dimensional anisotropy constant, $\bar{\phi}_{an}$, calculated in this study and by other authors. The value attributed to Gearheart was re-calculated [using Eq. (D2) of TG43U1 (Ref. 18)] to include their data from 1 cm that was not presented in their original paper but published later in Ibbott *et al.*'s letter to the editor (Ref. 25).

Seed name	Author	$\bar{\phi}_{an}$
STM12501	This study	0.940
	Kirov and Williamson ^j	0.941
Imagyn	This study	0.873
	Gearheart ^k	0.874
Theragenics	This study	0.871
	Monroe and Williamson ^l	0.866

^jReference 19.

^kReference 22.

^lReference 30.

likely due to residual voxel size effects in our calculations. The anisotropy factors and anisotropy constant all agree within 1%.

IV. CONCLUSION

In order to benchmark the new EGSnrc Monte Carlo code, BrachyDose, TG-43 dosimetry parameters were calculated for one ^{103}Pd and two ^{125}I sources. The three seeds in this study were chosen because of their varied internal structure and encapsulation. The STM ^{125}I and Theragenics ^{103}Pd seeds also make ideal candidates for benchmarking voxel based dose calculations due to their highly anisotropic dose distributions at small angles. Since the BrachyDose code is able to accurately calculate the dose distribution surrounding these two sources, we believe that, using the same voxel sizes as presented in this study, BrachyDose is capable of doing accurate dose calculations for any seed. A comprehensive set of dosimetry parameters is being calculated for the 16 seeds listed in the Joint AAPM/Radiological Physics Center (RPC) Registry of Brachytherapy Sources.³⁹

It was shown analytically that scoring the dose from a point source in 1-mm-thick spherical shells leads to a significant overestimate of dose at distances less than 1 cm from the source. To minimize voxel volume effects it was found that voxel sizes of $0.1 \times 0.1 \times 0.1 \text{ mm}^3$ were needed for points less than 1 cm from the source. From 1 to 5 cm away from the seed the voxel size was increased to $0.5 \times 0.5 \times 0.5 \text{ mm}^3$ and beyond 5 cm from the seed dose was scored in $1 \times 1 \times 1 \text{ mm}^3$ voxels. These voxel sizes should be suitable for doing calculations with other ^{125}I and ^{103}Pd seeds.

Cross section uncertainties play a significant role in calculations of the anisotropy function. Increasing the cross section of the titanium encapsulation for the Imagyn source by 1% resulted in a change of $\sim 0.5\%$ in the anisotropy function for $r < 1 \text{ cm}$ and $\theta < 15^\circ$. For the Theragenics source, decreasing the cross section of palladium by 5% resulted in an increase of $\sim 0.5\%$ in the anisotropy function for $\theta < 5^\circ$. Un-

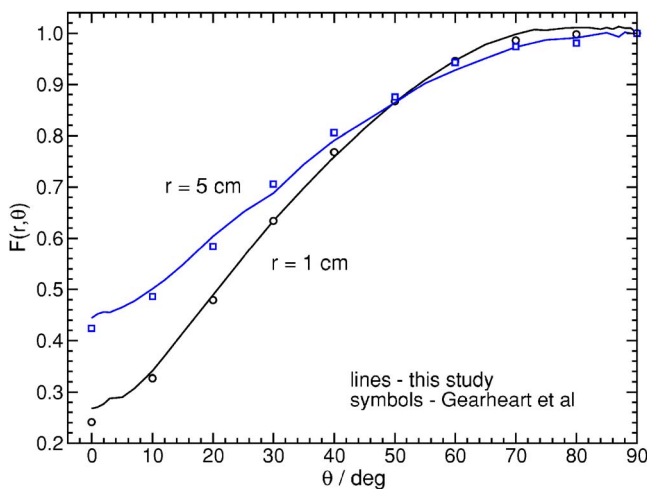


FIG. 10. Comparisons of anisotropy data calculated for the Imagyn isoStar ^{125}I source with values calculated by Gearheart *et al.* (Ref. 22). Voxel sizes are $(0.1 \text{ mm})^3$ at 1 cm and $(0.5 \text{ mm})^3$ at 5 cm.

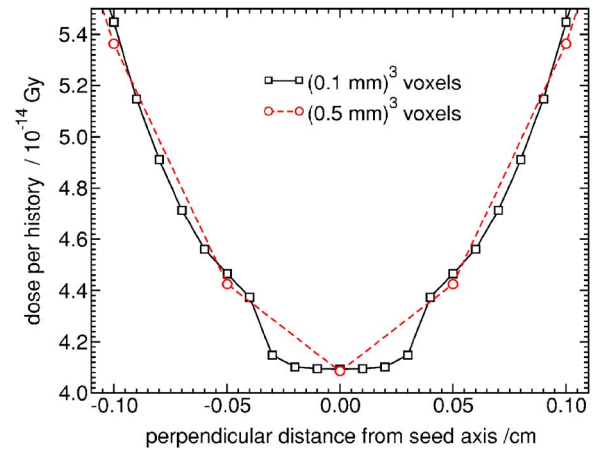


FIG. 11. Dose profile perpendicular to source axis located 0.5 cm from the Imagyn source center. Voxels are $(0.1 \text{ mm})^3$ and $(0.5 \text{ mm})^3$. It is evident from this plot that decreasing the voxel size further would likely have no effect on the anisotropy function values calculated at $\theta = 0^\circ$.

certainties in the geometry of the sources may also have a significant impact on calculated dosimetry parameters but have not been considered in this study. Combined uncertainties in cross sections and geometry are larger than the statistical uncertainties for the dosimetry parameters calculated in this study.

When voxel sizes are chosen appropriately, dosimetry parameters calculated with BrachyDose generally show good agreement with data calculated by other authors^{19,22,30} using Williamson's PTRAN^{13,14} code. This agreement demonstrates BrachyDose's ability to accurately calculate dose distributions surrounding brachytherapy seeds with widely varied internal structure and encapsulation.

Although the vast majority of our comparisons with previous data show good agreement, there are three cases where there are significant differences. First, the dose rate constant calculated for the STM source using the 2.7×2.7

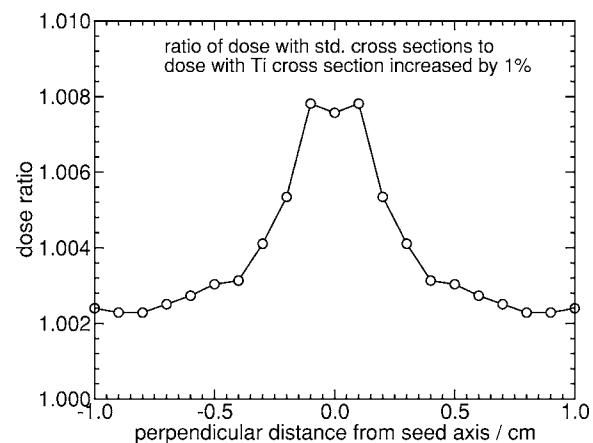


FIG. 12. For the Imagyn isoStar ^{125}I source, ratio of the dose calculated using the standard cross sections to dose calculated with the cross section of the Ti encapsulation increased by 1%. The dose ratio profile shown was taken perpendicular to the seed axis and 0.5 cm from the source center. A 1% increase in the cross section of titanium leads to a decrease in dose of 0.8% at 0° .

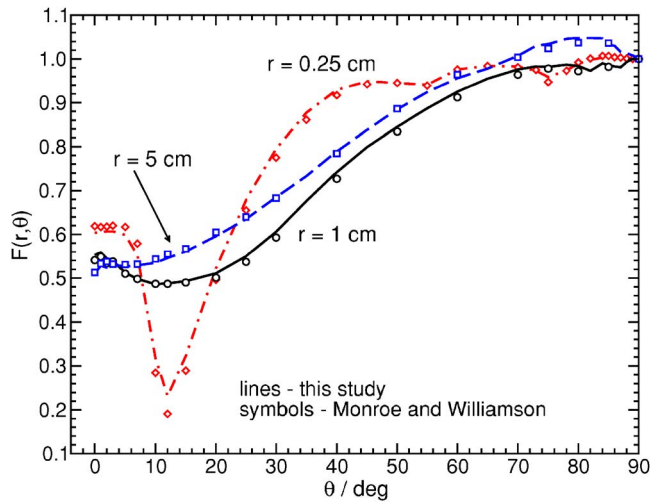


FIG. 13. Comparisons of anisotropy data calculated for the Theragenics Model 200 ^{103}Pd source with values calculated by Monroe and Williamson (Ref. 19). Voxel sizes are $(0.1\text{ mm})^3$ at 0.25 and 1 cm and $(0.5\text{ mm})^3$ at 5 cm.

$\times 0.05\text{ cm}^3$ voxel is 3.3% higher than the value calculated by Kirov and Williamson¹⁹ using a full simulation of the WAFAC. One might suspect that the more detailed model of the WAFAC explains the difference except that for the Theragenics seed our calculations agree very well with the more detailed calculations by Monroe and Williamson.³⁰ Second, BrachyDose calculated values of the radial dose function for the Theragenics seed show significant differences beyond 5 cm when compared with the results of Monroe and Williamson.³⁰ Finally, the anisotropy function calculated in this study for the Imagyn source shows significant differences at small angles when compared with the results of Gearheart *et al.*²² Given the consistency in our approach for the various seeds, we believe that our results are likely more accurate, but this remains to be established.

ACKNOWLEDGMENTS

We wish to thank Dr. Yang Cai for pointing out the useful equation [Eq. (7)] for calculating the angle β in the line source geometry function, as well as the members of the Carleton Laboratory for Radiotherapy Physics (CLRP) for their helpful comments regarding this paper. Many of the calculations in this study have made use of WestGrid computing resources, which are funded in part by the Canada Foundation for Innovation, Alberta Innovation and Science, BC Advanced Education, and the participating research institutions. This work is partially funded by NSERC, The Canada Research Chair's program and Varian Inc. The helpful comments of the referees are gratefully acknowledged.

^{a)}Electronic mail: rtaylor@physics.carleton.ca

^{b)}Electronic mail: drogers@physics.carleton.ca www: <http://www.physics.carleton.ca/~drogers/>

¹G. Yegin and D. W. O. Rogers, "A fast Monte Carlo code for multi-seed brachytherapy treatments including interseed effects," *Med. Phys.* **31**, 1771(abs) (2004).

²G. Yegin, R. E. P. Taylor, and D. W. O. Rogers, "BrachyDose: A new fast Monte Carlo code for brachytherapy calculations," *Med. Phys.* **33**, 2075–

2075(abs) (2006).

³I. Kawrakow, "Accurate condensed history Monte Carlo simulation of electron transport. I. EGSnrc, the new EGS4 version," *Med. Phys.* **27**, 485–498 (2000).

⁴I. Kawrakow and D. W. O. Rogers, "The EGSnrc code system: Monte Carlo simulation of electron and photon transport," Technical Report No. PIRS-701, National Research Council of Canada, Ottawa, Canada, 2000.

⁵C. Thomason, T. Mackie, M. Lindstrom, and P. Higgins, "The dose distribution surrounding Ir-192 and Cs-137 seed sources," *Phys. Med. Biol.* **36**, 475–493 (1991).

⁶G. Luxton, "Comparison of radiation-dosimetry in water and in solid phantom materials for I-125 and Pd-103 brachytherapy sources - EGS4 Monte Carlo study," *Med. Phys.* **21**, 621–641 (1994).

⁷R. Wang and R. S. Sloboda, "EGS4 dosimetry calculations for cylindrically symmetric brachytherapy sources," *Med. Phys.* **23**, 1459–1465 (1996).

⁸E. Mainegra, R. Capote, and E. Lopez, "Dose rate constants for ^{103}Pd , ^{125}I , ^{196}Yb , ^{192}Ir , brachytherapy sources: An EGS4 Monte Carlo study," *Phys. Med. Biol.* **43**, 1557–1566 (1998).

⁹G. Luxton and G. Jozsef, "Radial dose distribution, dose to water and dose rate constant for monoenergetic photon point sources from 10 keV to 2 MeV: EGS4 Monte Carlo model calculation," *Med. Phys.* **26**, 2531–2538 (1999).

¹⁰E. Mainegra, R. Capote, and E. Lopez, "Radial dose functions for ^{103}Pd , ^{125}I , ^{196}Yb , ^{192}Ir , brachytherapy sources: An EGS4 Monte Carlo study," *Phys. Med. Biol.* **45**, 703–717 (2000).

¹¹R. Capote, E. Mainegra, and E. Lopez, "Anisotropy functions for low energy interstitial brachytherapy sources: An EGS4 Monte Carlo study," *Phys. Med. Biol.* **46**, 135–150 (2001).

¹²R. Wang and X. Li, "A Monte Carlo calculation of dosimetric parameters of Sr-90/Y-90 and Ir-192 SS sources for intravascular brachytherapy," *Med. Phys.* **27**, 2528–2535 (2000).

¹³J. F. Williamson, "Comparison of measured and calculated dose rates in water near I-125 and Ir-192 seeds," *Med. Phys.* **18**, 776–786 (1991).

¹⁴J. F. Williamson, "Monte Carlo evaluation of kerma at a point for photon transport problems," *Med. Phys.* **14**, 567–576 (1987).

¹⁵T. Rusch, T. Bohm, and M. Rivard, "Monte Carlo modeling of the Xofig AXXENT x-ray source," *Med. Phys.* **32**, 2017–2018(abs) (2005).

¹⁶Mark J. Rivard, Stephen D. Davis, Larry A. DeWerd, Thomas W. Rusch, and Steve Alexrod, "Calculated and measured brachytherapy dosimetry parameters in water for the Xofig Axxent X-Ray Source: An electronic brachytherapy source," *Med. Phys.* **33**, 4020–4032 (2006).

¹⁷R. Nath, L. L. Anderson, G. Luxton, K. A. Weaver, J. F. Williamson, and A. S. Meigooni, "Dosimetry of interstitial brachytherapy sources: Recommendations of the AAPM Radiation Therapy Committee Task Group No. 43," *Med. Phys.* **22**, 209–234 (1995).

¹⁸M. J. Rivard, B. M. Coursey, L. A. DeWerd, M. S. Huq, G. S. Ibbott, M. G. Mitch, R. Nath, and J. F. Williamson, "Update of AAPM Task Group No. 43 Report: A revised AAPM protocol for brachytherapy dose calculations," *Med. Phys.* **31**, 633–674 (2004).

¹⁹A. S. Kirov and J. F. Williamson, "Monte Carlo-aided dosimetry of the Source Tech Medical Model STM1251 I-125 interstitial brachytherapy source," *Med. Phys.* **28**, 764–772 (2001).

²⁰Z. Li and J. F. Williamson, "Measured transverse-axis dosimetric parameters of the model STM1251 ^{125}I interstitial source," *J. Appl. Clin. Med. Phys.* **3**, 212–217 (2002).

²¹S. Chiu-Tsao, T. L. Duckworth, C. Hsiung, Z. Li, J. Williamson, N. Patel, and L. B. Harrison, "Thermoluminescent dosimetry of the SourceTech Medical model STM1251 ^{125}I seed," *Med. Phys.* **30**, 1735–1732 (2003).

²²D. M. Gearheart, A. Drogin, K. Sowards, A. Meigooni, and G. S. Ibbott, "Dosimetric characteristics of a new ^{125}I brachytherapy source," *Med. Phys.* **27**, 2278–2285 (2000).

²³R. Nath and N. Yue, "Dose distribution along the transverse axis of a new ^{125}I source for interstitial brachytherapy," *Med. Phys.* **27**, 2536–2540 (2000).

²⁴G. S. Ibbott and R. Nath, "Dose-rate constant for Imagyn ^{125}I brachytherapy source," *Med. Phys.* **28**, 705 (2001).

²⁵G. S. Ibbott, "Monte Carlo determination of dose rate constant," *Med. Phys.* **29**, 1637–1638 (2002).

²⁶Z. Chen and R. Nath, "Dose rate constant and energy spectrum of interstitial brachytherapy sources," *Med. Phys.* **28**, 86–96 (2001).

²⁷J. F. Williamson, "Monte Carlo modeling of the transverse-axis dose distribution of the Model 200 ^{103}Pd interstitial brachytherapy source," *Med.*

- Phys. **27**, 643–654 (2000).
- ²⁸R. Nath, N. Yue, K. Shahnazi, and P. Bongiorini, “Measurement of dose-rate constant for ^{103}Pd seeds with air kerma strength calibration based upon a primary national standard,” *Med. Phys.* **27**, 655–658 (2000).
- ²⁹G. Yegin, “A new approach to geometry modeling of Monte Carlo particle transport: An application to EGS,” *Nucl. Instrum. Methods Phys. Res. B* **211**, 331–338 (2003).
- ³⁰J. I. Monroe and J. F. Williamson, “Monte Carlo-aided dosimetry of the Theragenics TheraSeed Model 200 ^{103}Pd interstitial brachytherapy seed,” *Med. Phys.* **29**, 609–621 (2002).
- ³¹M. J. Berger and J. H. Hubbell, XCOM: Photon cross sections on a personal computer, Report No. NBSIR87–3597, NIST, Gaithersburg, MD 20899 (1987).
- ³²C. S. Melhus and M. J. Rivard, “Approaches to calculating AAPM TG-43 brachytherapy dosimetry parameters for ^{137}Cs , ^{125}I , ^{192}Ir , ^{103}Pd , and ^{169}Yb sources,” *Med. Phys.* **33**, 1729–1737 (2006).
- ³³I. Kawrakow, “On the effective point of measurement in megavoltage photon beams,” *Med. Phys.* **33**, 1829–1839 (2006).
- ³⁴R. Loevinger, “Wide-angle free-air chamber for calibration of low-energy brachytherapy sources,” *Med. Phys.* **20**, 907 (1993).
- ³⁵S. M. Seltzer, P. J. Lamperti, R. Loevinger, M. G. Mitch, J. T. Weaver, and B. M. Coursey, “New national air-kerma-strength standards for ^{125}I and ^{103}Pd Brachytherapy seeds,” *J. Res. Natl. Inst. Stand. Technol.* **108**, 337–358 (2003).
- ³⁶S. D. Davis, C. K. Ross, P. N. Mobit, L. Van der Zwan, W. J. Chase, and K. R. Shortt, “The response of LiF TLDs to photon beams in the energy range from 30 kV to ^{60}Co γ -rays,” *Radiat. Prot. Dosim.* **106**, 33–44 (2003).
- ³⁷R. K. Das, Z. Li, H. Perera, and J. F. Williamson, “Accuracy of Monte Carlo photon transport simulation in characterizing brachytherapy dosimeter energy-response artifacts,” *Phys. Med. Biol.* **41**, 995–1006 (1996).
- ³⁸R. W. Roussin, J. R. Knight, J. H. Hubbell, and R. J. Howerton, “Description of the DLC-99/HUGO package of photon interactions,” RSIC Data Library Collection, Report No. ORNL-RSIC-46, Radiation Shielding Information Center, Oak Ridge National Laboratory, Oak Ridge, Tennessee (1983).
- ³⁹Radiological Physics Center, “The joint AAPM/RPC registry of brachytherapy sources,” The M.D. Anderson Cancer Center, Houston Texas (see <http://rpc.mdanderson.org/rpc/>).